Applied Physics Letters ARTICLE scitation.org/journal/apl

Optical and electrical properties of two-dimensional palladium diselenide

Cite as: Appl. Phys. Lett. **114**, 253102 (2019); doi: 10.1063/1.5097825
Submitted: 28 March 2019 · Accepted: 10 June 2019 ·
Published Online: 24 June 2019

George Zhang,[1,2] Matin Amani,[1,2] Apoorva Chaturvedi,[3] Chaoliang Tan,[1,2] James Bullock,[1,2] Xiaohui Song,[4,5] Hyungjin Kim,[1,2] Der-Hsien Lien,[1,2] Mary C. Scott,[4,5] Hua Zhang,[3,6] and Ali Javey[1,2,a)]

AFFILIATIONS

[1]Electrical Engineering and Computer Sciences, University of California at Berkeley, Berkeley, California 94720, USA
[2]Materials Sciences Division, Lawrence Berkeley National Laboratory, Berkeley, California 94720, USA
[3]Center for Programmable Materials, School of Materials Science and Engineering, Nanyang Technological University, Block N4.1, 50 Nanyang Avenue, 639798 Singapore
[4]Materials Science and Engineering, University of California at Berkeley, Berkeley, California 94720, USA
[5]The Molecular Foundry, Lawrence Berkeley National Laboratory, Berkeley, California 94720, USA
[6]Department of Chemistry, City University of Hong Kong, Kowloon, Hong Kong, China

[a)]Author to whom correspondence should be addressed: ajavey@eecs.berkeley.edu

ABSTRACT

Two-dimensional (2D) noble-metal dichalcogenides exhibit exceptionally strong thickness-dependent bandgaps, which can be leveraged in a wide variety of device applications. A detailed study of their optical (e.g., optical bandgaps) and electrical properties (e.g., mobilities) is important in determining potential future applications of these materials. In this work, we perform detailed optical and electrical characterization of 2D $PdSe_2$ nanoflakes mechanically exfoliated from a single-crystalline source. Layer-dependent bandgap analysis from optical absorption results indicates that this material is an indirect semiconductor with bandgaps of approximately 1.37 and 0.50 eV for the monolayer and bulk, respectively. Spectral photoresponse measurements further confirm these bandgap values. Moreover, temperature-dependent electrical measurements of a 6.8-nm-thick $PdSe_2$ flake-based transistor show effective electron mobilities of 130 and 520 $cm^2 V^{-1} s^{-1}$ at 300 K and 77 K, respectively. Finally, we demonstrate that $PdSe_2$ can be utilized for short-wave infrared photodetectors. A room-temperature specific detectivity (D^*) of 1.8×10^{10} cm $Hz^{1/2}$ W^{-1} at 1 μm with a band edge at 1.94 μm is achieved on a 6.8-nm-thick $PdSe_2$ flake-based photodetector.

Two-dimensional (2D) transition metal dichalcogenides (TMDCs) have attracted considerable attention and have been explored for numerous applications including electronics, optoelectronics, catalysis, and sensors in the last decade.[1] Motivated by the attractive properties and wide applications of TMDCs, researchers have explored other 2D two-element systems including the 2D noble-metal dichalcogenides (NMDCs) with the general formula MX_2 (where M = Pt, Pd and X = S, Se, Te).[2] NMDCs have recently been synthesized and demonstrated to exhibit air stability and strongly thickness-dependent bandgaps. For example, $PtSe_2$ and PdS_2 exhibit a sharp thickness-modulated semiconductor-to-metal transition,[3–5] whereas PtS_2 also shows a strong thickness dependence but is a narrow-bandgap indirect semiconductor in bulk.[6] Both $PtTe_2$ and $PdTe_2$ are semimetals,[7,8] with the latter exhibiting superconductivity.[9,10]

Palladium diselenide ($PdSe_2$), a NMDC, has also been synthesized and explored in the last few years. Field-effect transistors (FETs) based on $PdSe_2$ flakes show electron mobilities up to ~200 $cm^2 V^{-1} s^{-1}$.[11] $PdSe_2$ was experimentally reported to have a thickness-dependent bandgap, in which monolayer $PdSe_2$ has a bandgap of ~1.4 eV and bulk $PdSe_2$ is metallic with a bandgap approaching 0 eV.[12] More recently, $PdSe_2$ has been investigated for infrared detectors.[13] In this work, we systematically study the optical and electrical properties of $PdSe_2$ with an emphasis on its thickness-dependent bandgap to determine future applications of this material. Our results show that $PdSe_2$ is an indirect semiconductor with a monolayer bandgap of 1.37 eV and a bulk bandgap of 0.5 eV (in contrast to previous works which have predicted metallic bulk), as shown by optical absorption and photoresponse measurements. Furthermore, the temperature-dependent electrical

measurements of a 6.8-nm-thick $PdSe_2$ flake-based transistor show effective electron mobilities of 130 and 520 $cm^2\ V^{-1}\ s^{-1}$ at 300 K and 77 K, respectively. Owing to its relatively small bandgap, thick $PdSe_2$ can be utilized for short-wave infrared (SWIR) photodetectors. A room-temperature peak specific detectivity (D^*) of 6.4×10^{10} cm $Hz^{1/2}$ W^{-1} at 0.7 μm with a band edge at 1.94 μm is achieved on a 6.8-nm-thick $PdSe_2$ flake-based photodetector.

The crystal structure of $PdSe_2$ is shown in Figs. 1(a) and 1(b). $PdSe_2$ is a layered 2D material with a theoretical monolayer thickness of ~4.8 Å. $PdSe_2$ also has pentagonal-structured layers,[11,12] as shown in Fig. 1(b). Pentagonal 2D materials have been theoretically proposed[14,15] although $PdSe_2$ has been synthesized and experimentally characterized as a 2D material. Figure 1(c) shows the measured X-ray diffraction (XRD) pattern of a bulk $PdSe_2$ crystal grown by chemical vapor transport (CVT), which is consistent with the simulated XRD pattern, confirming the synthesis of bulk single crystal $PdSe_2$. 2D $PdSe_2$ nanoflakes of varying thicknesses were mechanically exfoliated from a large single-crystalline source. Figure 1(d) shows the Raman spectra of $PdSe_2$ flakes of thicknesses ranging from monolayer to bulk. The locations of the Raman modes A_g^1-B_{g1}^1, A_g^2, B_{g1}^2, A_g^3, and B_{g1}^3 and their shifts with the changing thickness are consistent with previous reports on $PdSe_2$.[12] Figure 1(e) shows the high-resolution transmission electron microscopy (HR-TEM) image of a 6.8-nm-thick $PdSe_2$ flake. The lattice constant is 0.29 nm, which can be assigned to the (200) planes of the $PdSe_2$ single crystal. The corresponding selected area electron diffraction (SAED) pattern shows a single set of bright diffraction dots [Fig. 1(f)], further confirming the single crystalline nature.

To perform optical measurements, $PdSe_2$ flakes were exfoliated onto quartz by mechanical exfoliation and gold-mediated exfoliation,[16] which can yield large-area mono- and few-layer $PdSe_2$ flakes. Optical transmittance and reflectance measurements were conducted using both a UV-Vis microabsorption setup and a Fourier-transform infrared microscope. The combination of these techniques permits measurements over a wavelength range of 450 nm–15 μm.[17] UV-Vis measurements were performed with reference to a blank quartz substrate and a silver mirror [Figs. 2(a) and 2(b)], while FTIR measurements were performed with reference to a blank quartz or KBr substrate and a gold mirror [Figs. 2(c) and 2(d)]. Quartz is optically transparent for visible to SWIR wavelengths, whereas the transparency of KBr extends further a few microns beyond long-wave infrared (LWIR) wavelengths. Note that the reflectance and transmittance of thick $PdSe_2$ flakes show out-of-phase oscillations due to multiple reflections occurring in the 2D film; this destructive and constructive interference behavior is accounted for when calculating the absorption coefficient, as shown more clearly in Fig. S1 in the supplementary material. We did not observe differences in transmittance and reflectance of $PdSe_2$ flakes prepared by mechanical exfoliation and gold-mediated exfoliation. To account for thin-film interference in the $PdSe_2$ flake, we used the transfer matrix method. For transmission and reflection of light by a thin film on a substrate, we define the Fresnel coefficients[18]

$$r_1 = \frac{n_0 - n_1}{n_0 + n_1}, \quad t_1 = \frac{2n_0}{n_0 + n_1}, \\ r_2 = \frac{n_1 - n_2}{n_1 + n_2}, \quad t_2 = \frac{2n_1}{n_1 + n_2}, \tag{1}$$

where $n_0 = 1.00$, $n_1 = n - ik$, and $n_2 = 1.46$ are the refractive indices of air, the $PdSe_2$ flake, and quartz, respectively. The reflected and transmitted amplitudes are

$$R = \frac{r_1 + r_2 e^{-2i\delta_1}}{1 + r_1 r_2 e^{-2i\delta_1}}, \quad T = \frac{t_1 t_2 e^{-i\delta_1}}{1 + r_1 r_2 e^{-2i\delta_1}}, \tag{2}$$

where $\delta_1 = (2\pi/\lambda) n_1 d_1$ and d_1 is the thickness of the $PdSe_2$ flake.[18] The reflectance and transmittance as ratios of the energy reflected and transmitted to the energy incident are[18]

$$\boldsymbol{R}_{\mathrm{sim}} = RR^*, \quad \boldsymbol{T}_{\mathrm{sim}} = \frac{n_2}{n_0} TT^*. \tag{3}$$

We then used the Nelder-Mead algorithm to minimize $(\boldsymbol{R}_{\mathrm{meas}} - \boldsymbol{R}_{\mathrm{sim}})^2 + (\boldsymbol{T}_{\mathrm{meas}} - \boldsymbol{T}_{\mathrm{sim}})^2$ to estimate the complex refractive index, $n_1 = n - ik$, of the $PdSe_2$ flake.[19,20] Finally, we extracted the optical bandgap of the $PdSe_2$ flake from a Cody plot of $(\alpha/h\nu)^{1/2}$ vs $h\nu$, where

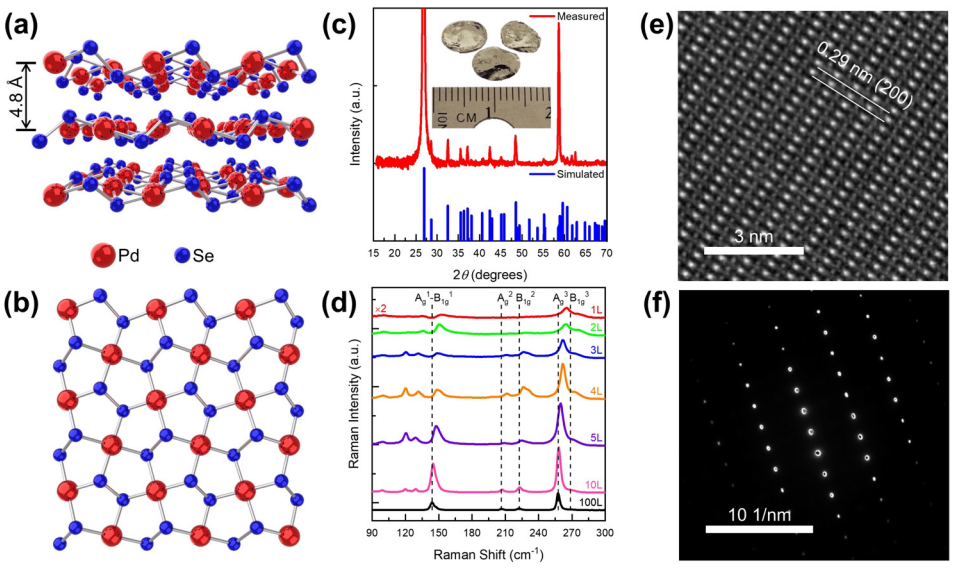

FIG. 1. Crystal structure of $PdSe_2$: (a) lateral and (b) top-down view. (c) Measured and simulated XRD spectra of a bulk $PdSe_2$ crystal. (d) Raman spectra of $PdSe_2$ for various thicknesses. (e) HR-TEM image and (f) SAED pattern of a 6.8-nm-thick $PdSe_2$ flake.

$\alpha = 4\pi k/\lambda$ is the absorption coefficient of the $PdSe_2$ flake,[19] as shown in Fig. 2(e) for $PdSe_2$ flakes of varying thicknesses. The optical microscopy images of these flakes along with their thicknesses measured via atomic force microscopy (AFM) are shown in Fig. S2 in the supplementary material. Figure 2(f) shows the measured optical indirect bandgap of $PdSe_2$ as a function of its thickness, which agrees with theoretical calculations in terms of the monolayer bandgap, but deviates from previously reported experimental data in terms of the bulk bandgap.[12] This experimental deviation is likely due to both accounting for thickness-dependent reflectance (in addition to thickness-dependent transmittance) and the broader spectral range (~0.35–3.1 eV) measured in this work, which fully encompasses the bandgap range of $PdSe_2$. A previous work on $PdSe_2$ extrapolated optical bandgap values from a measured spectral range of ~1.3–3.25 eV, which is nearly a whole electron volt beyond the bulk bandgap of $PdSe_2$.[12] Accounting for thin-film interference only changes the bandgap by ~0.1 eV (supplementary material Fig. S1),[12] whereas neglecting reflectance and extrapolating far beyond the bandgap can drastically alter the bandgap value (supplementary material Fig. S3). This can be clearly seen for reflection and transmission measurements performed on a 134-nm-thick $PdSe_2$ flake which shows an absorption edge around 2 μm (supplementary material Fig. S4).

Using electron-beam lithography, back-gated $PdSe_2$ field-effect transistors (FETs) were fabricated on 90 nm SiO_2/Si with 100-nm-thick nickel (Ni) contacts. The device structure and optical microscopy images of fabricated devices are shown in Fig. 3(a). Figure 3(b) shows the temperature-dependent I_d-V_g characteristics of the 6.8-nm-thick $PdSe_2$ device measured at a low drain voltage V_d of 10 mV, indicating that the on/off ratio increases as temperature decreases. The inset shows a plot of the same data on the linear-I_d scale, clearly showing that the drain-source current $I_{d,max}$ increases with decreasing temperature. We can therefore expect the mobility of this 6.8-nm-thick $PdSe_2$ flake to reach its maximum at low temperatures. I_d-V_g shows ambipolar conduction since the onset of n-type and p-type conduction is roughly centered around $V_g = 0$ V, suggesting that the material is roughly intrinsic (i.e., low background doping). The ambipolar characteristics of $PdSe_2$ can be drastically tuned by introducing molecular dopants to $PdSe_2$ while annealing under vacuum.[11] The same temperature-dependent I_d-V_g plot is shown in Fig. S5 in the supplementary material but with a second measurement of the device at $T = 300$ K taken after 9 months of storage in nitrogen and ambient air, demonstrating the air stability of $PdSe_2$. From linear-I_d-V_g plots, we extrapolate room-temperature threshold voltages V_t of 2.25 V and 4.45 V for the 6.8-nm- and 116-nm-thick $PdSe_2$ devices, respectively.

Figure 3(c) shows the I_d-V_d characteristics of the 6.8-nm-thick $PdSe_2$ device inset with those of the 116-nm-thick $PdSe_2$ device. Since the drain saturation voltage $V_{d,sat} = V_g - V_t$ exceeds the range of measurements, we do not observe saturation. Additionally, the linear behavior of the I_d-V_d characteristics at low values of V_d suggests minimal contact resistance with small Schottky barrier heights. From these transfer characteristics, we calculated the effective electron mobility, $\mu_{eff} = (dI_d/dV_d)(L_g/w_c)[C_{ox}(V_g - V_t - 0.5\,V_d)]^{-1}$, and field-effect electron mobility, $\mu_{fe} = (dI_d/dV_g)(L_g/w_c)(C_{ox}V_d)^{-1}$, of the 6.8-nm-thick $PdSe_2$ device vs temperature, as shown in Fig. 3(d). The electron mobility of the 6.8-nm-thick $PdSe_2$ device increases with decreasing temperature. The 6.8-nm-thick $PdSe_2$ device exhibits effective electron mobilities of 130 and 520 $cm^2\,V^{-1}\,s^{-1}$ at 300 K and 77 K, respectively. We can fit the temperature-dependent mobility of this device with a power law, $\mu_{eff} \propto T^{-\gamma}$, where $\gamma = 1.08$, suggesting that the mobility is limited by phonon scattering.[21,22] Finally, we extracted a lower bound on the bandgap of a 6.8-nm-thick $PdSe_2$ flake from an Arrhenius plot of the minimum drain-source current $I_{d,min}$ vs the inverse of temperature T by using

$$I_{d,min} \propto \exp(-E_g/2kT), \tag{4}$$

where E_g is the transport bandgap and k is the Boltzmann constant [Fig. 3(e)]. We extract a bandgap of 0.57 eV for a 6.8-nm-thick $PdSe_2$ flake. Due to the contribution from trap states, this method is expected to underestimate the bandgap.[23] Finally, to further confirm the optical measurements shown in Fig. 2(f), we performed temperature-dependent measurements on a $PdSe_2$ transistor fabricated using a bulk (116-nm-thick) crystal, as shown in Fig. 3(f). Since the thickness of this device is significantly greater than the Debye screening length, the device cannot be fully turned off. Nevertheless, we still observe

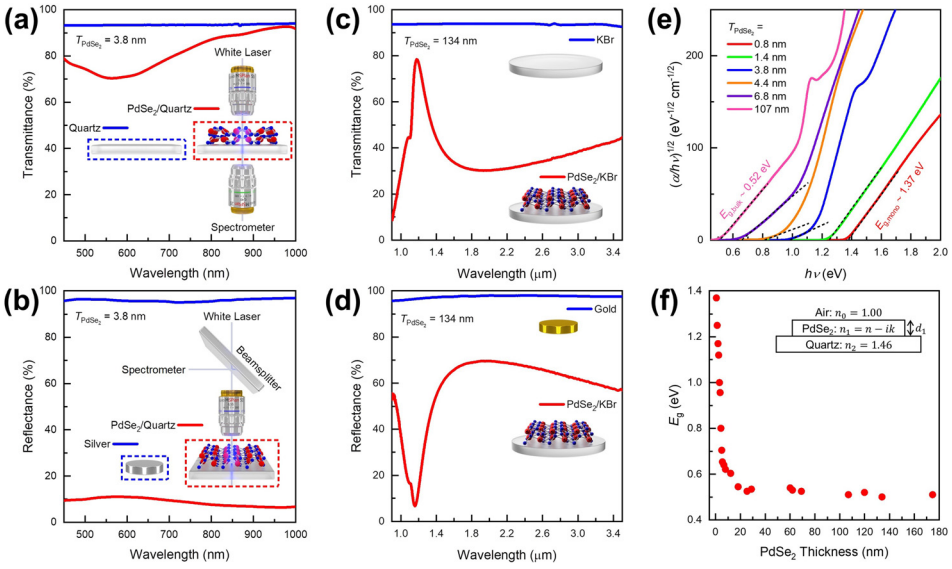

FIG. 2. (a) Transmission and (b) reflection measurements of a 3.8-nm-thick $PdSe_2$ flake on a quartz substrate in the visible-wavelength range. (c) Transmission and (d) reflection measurements of a 134-nm-thick $PdSe_2$ flake on a KBr substrate in the infrared-wavelength range. (e) Optical indirect bandgap extraction of $PdSe_2$ for various thicknesses. (f) Optical indirect bandgap of $PdSe_2$ as a function of its thickness.

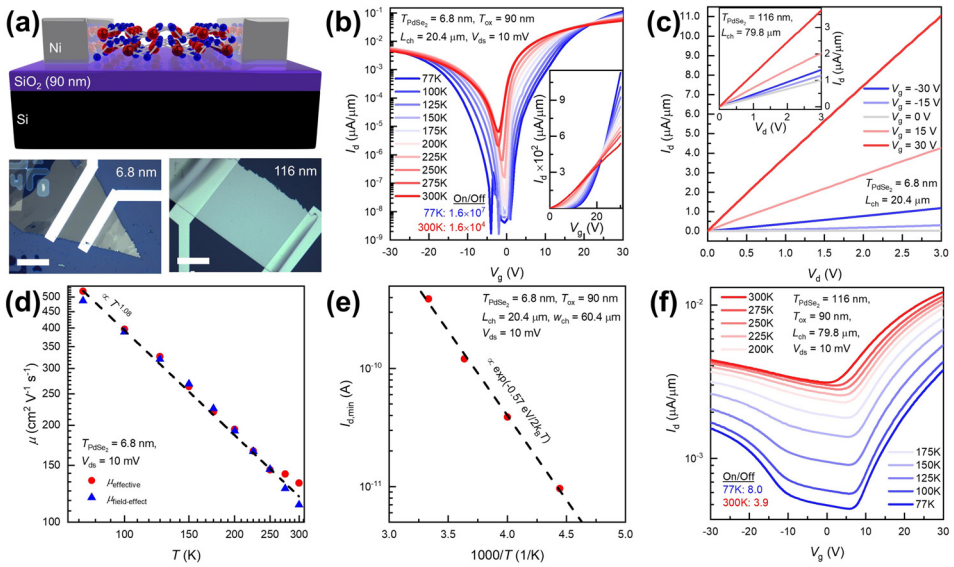

FIG. 3. (a) Back-gated $PdSe_2$ field-effect transistor (FET) structure and optical microscopy images of devices with 6.8-nm- and 116-nm-thick $PdSe_2$ flakes. Scale bars are 30 μm. (b) Temperature-dependent I_d-V_g characteristics of the 6.8-nm-thick $PdSe_2$ device measured at a low V_d value of 10 mV. The inset shows a plot of the same data on the linear-I_d scale. (c) I_d-V_d characteristics of the 6.8-nm-thick $PdSe_2$ device inset with those of the 116-nm-thick $PdSe_2$ device. (d) Effective and field-effect mobility of the 6.8-nm-thick $PdSe_2$ device. The dashed line shows a power law fit $\mu_{effective} \propto T^{-\gamma}$, where $\gamma = 1.08$. (e) Arrhenius plot showing the minimum drain-source current ($I_{d,min}$) of the 6.8-nm-thick $PdSe_2$ device as a function of temperature to extract the transport bandgap $E_g = 0.57$ eV. (f) Temperature-dependent I_d-V_g of the 116-nm-thick $PdSe_2$ device measured at $V_d = 10$ mV, showing bulk semiconducting behavior.

moderate gate-dependent transport due to the low background doping in $PdSe_2$. This indicates that bulk $PdSe_2$ is semiconducting and is consistent with the absorption measurements shown above.

We next investigate the performance of $PdSe_2$ as a photoconductor utilizing the devices discussed in Fig. 3. Figure 4(a) shows the room-temperature spectral responsivities of the 6.8-nm- and 116-nm-thick $PdSe_2$ devices shown in Fig. 3(a). We measured the spectral responsivity of these devices using an FTIR by replacing the internal detector with the $PdSe_2$ devices and focusing its light source on the devices with a CaF_2 lens. The internal deuterated triglycine sulfate (DTGS) in the FTIR was used to find the relative intensity of the light source and a NIST-traceable Ge photodiode to calibrate the illumination intensity of the light source.[24] The responsivity is calculated as $R(\lambda) = I_{ph}(\lambda)/P_{in}(\lambda)$, where I_{ph} is the photocurrent and P_{in} is the incident power on the device. The specific detectivity (D^*) is then calculated using

$$D^* = \frac{\sqrt{A\Delta f}}{\mathrm{NEP}} = \frac{R\sqrt{A\Delta f}}{i_n}, \tag{5}$$

where A is the device area, Δf is the integration time, NEP is the noise equivalent power, and $i_n 2 = 2qI_d\Delta f$ is the squared noise current, where I_d is the dark current. Figure 4(b) shows the room-temperature spectral D^* of the 6.8-nm- and 116-nm-thick $PdSe_2$ devices. We find a room-temperature D^* value of 1.8×10^{10} cm $Hz^{1/2}$ W^{-1} at a wavelength of 1 μm for the 6.8-nm-thick $PdSe_2$ device. From a plot of $(EQE/h\nu)^{1/2}$ vs $h\nu$, where EQE is the external quantum efficiency we extracted 0.59 eV and 0.49 eV as the optical bandgaps for a 6.8-nm- and 116-nm-thick $PdSe_2$ flake, respectively [Figs. 4(c) and 4(d)]. It is important to note that the photoresponse measurements shown were taken at $V_g = 0$. This was found to give the highest photoresponse and is consistent with the I_d-V_g characteristics which show the lowest dark current for V_g near zero.

In conclusion, we have performed a systematic study on the optical and electrical properties of $PdSe_2$, a layered two-dimensional

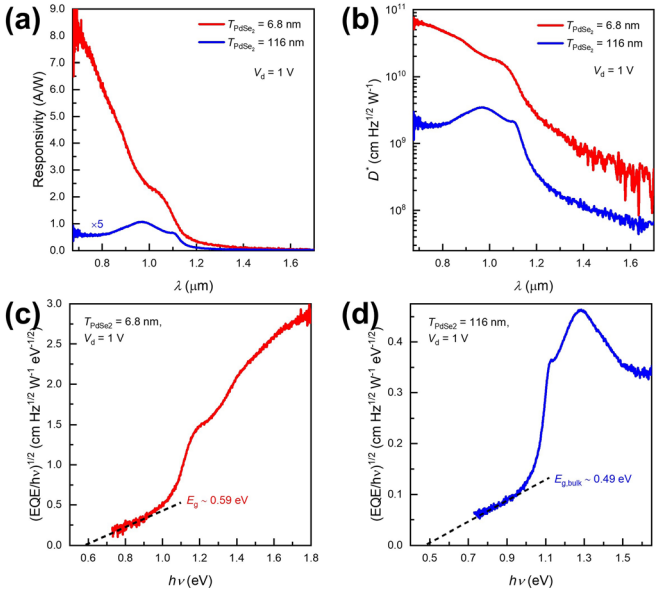

FIG. 4. (a) Room-temperature spectral responsivities and (b) specific detectivities D^* of the 6.8-nm- and 116-nm-thick $PdSe_2$ devices shown in Fig. 3(a) measured at a drain voltage V_d of 1 V with zero gate voltage V_g applied. (c) and (d) Indirect bandgap extraction of a 6.8-nm-thick and a 116-nm-thick $PdSe_2$ flake.

pentagonal semiconductor with an indirect bandgap ranging from ~0.5 to 1.37 eV. We found that a 6.8-nm-thick $PdSe_2$ flake-based transistor has effective electron mobilities of 130 and 520 $cm^2\ V^{-1}\ s^{-1}$ at 300 K and 77 K, respectively. The same transistor can serve as a SWIR photoconductive detector with a D^* value of 1.88×10^{10} cm $Hz^{1/2}\ W^{-1}$ at 1 μm with a cutoff wavelength of 1.94 μm. At 1 μm, $PdSe_2$ has a D^* value on the same order of magnitude as 2D tellurium (Te)[23] and black phosphorous (bP).[24] Te and bP, however, have optimized cutoff wavelengths of 3.4 μm and 4.6 μm, respectively, allowing more coverage of the SWIR band compared to $PdSe_2$. Nonetheless, given the promising preliminary values of D^* for our simple $PdSe_2$ device structure, further optimization, e.g., optical cavity substrate engineering to shift the peak D^* and cutoff wavelength, may allow the use of $PdSe_2$ for high-performance SWIR photodetectors.[23] Most importantly, through different measurements, we have determined that $PdSe_2$ does not undergo a semiconductor to metal transition with the increasing thickness. This finding changes the outlook of the potential application space in which $PdSe_2$ may be used without further manipulating the material's band structure, e.g., by strain[25,26] or defect[27] engineering.

See the supplementary material for additional material characterization.

Device fabrication and measurements were supported by the Defense Advanced Research Projects Agency under Contract No. HR0011-16-1-0004. Synthesis work was supported by the U.S. Department of Energy, Office of Science, Office of Basic Energy Sciences, Materials Sciences and Engineering Division under Contract No. DE-AC02-05CH11231 within the Electronic Materials Program (KC1201). The work at the Molecular Foundry was supported by the Office of Science, Office of Basic Energy Sciences, of the U.S. Department of Energy under Contract No. DE-AC02-05CH11231. H.Z. thanks the support from ITC via the Hong Kong Branch of National Precious Metals Material Engineering Research Center and the Start-Up Grant from the City University of Hong Kong.

REFERENCES

[1]C. L. Tan, X. H. Cao, X.-J. Wu, Q. Y. He, J. Yang, X. Zhang, J. Z. Chen, W. Zhao, S. K. Han, G.-H. Nam, M. Sindoro, and H. Zhang, "Recent advances in ultrathin two-dimensional nanomaterials," Chem. Rev. **117**, 6225–6331 (2017).
[2]P. Miró, M. Ghorbani-Asl, and T. Heine, "Two dimensional materials beyond MoS_2: Noble-transition-metal dichalcogenides," Angew. Chem. **53**, 3015–3018 (2014).
[3]A. Ciarrocchi, A. Avsar, D. Ovchinnikov, and A. Kis, "Thickness-modulated metal-to-semiconductor transformation in a transition metal dichalcogenide," Nat. Commun. **9**, 919 (2018).
[4]Y. Zhao, J. Qiao, Z. Yu, P. Yu, K. Xu, S. P. Lau, W. Zhou, Z. Liu, X. Wang, W. Ji, and Y. Chai, "High-electron-mobility and air-stable 2D layered $PtSe_2$ FETs," Adv. Mater. **29**, 1604230 (2017).
[5]M. Ghorbani-Asl, A. Kuc, P. Miró, and T. Heine, "A single-material logical junction based on 2D crystal PdS_2," Adv. Mater. **28**, 853–856 (2016).
[6]Y. Zhao, J. Qiao, P. Yu, Z. Hu, Z. Lin, S. P. Lau, Z. Liu, W. Ji, and Y. Chai, "Extraordinarily strong interlayer interaction in 2D layered PtS_2," Adv. Mater. **28**, 2399–2407 (2016).
[7]M. Yan, H. Huang, K. Zhang, E. Wang, W. Yao, K. Deng, G. Wan, H. Zhang, M. Arita, H. Yang, Z. Sun, H. Yao, Y. Wu, S. Fan, W. Duan, and S. Zhou, "Lorentz-violating type-II Dirac fermions in transition metal dichalcogenide $PtTe_2$," Nat. Commun. **8**, 257 (2017).
[8]H. Ma, P. Chen, B. Li, J. Li, R. Ai, Z. Zhang, G. Sun, K. Yao, Z. Lin, B. Zhao, R. Wu, X. Tang, X. Duan, and X. Duan, "Thickness-tunable synthesis of ultrathin type-II Dirac semimetal $PtTe_2$ single crystals and their thickness-dependent electronic properties," Nano Lett. **18**, 3523–3529 (2018).
[9]O. J. Clark, M. J. Neat, K. Okawa, L. Bawden, I. Marković, F. Mazzola, J. Feng, V. Sunko, J. M. Riley, W. Meevasana, J. Fujii, I. Vobornik, T. K. Kim, M. Hoesch, T. Sasagawa, P. Wahl, M. S. Bahramy, and P. D. C. King, "Fermiology and superconductivity of topological surface states in $PdTe_2$," Phys. Rev. Lett. **120**, 156401 (2018).
[10]S. Das, Amit, A. Sirohi, L. Yadav, S. Gayen, Y. Singh, and G. Sheet, "Conventional superconductivity in the type-II Dirac semimetal $PdTe_2$," Phys. Rev. B **97**, 014523 (2018).
[11]W. L. Chow, P. Yu, F. Liu, J. Hong, X. Wang, Q. Zeng, C.-H. Hsu, C. Zhu, J. Zhou, X. Wang, J. Xia, J. Yuan, Y. Chen, D. Wu, T. Yu, Z. Shen, H. Lin, C. Jin, B. K. Tay, and Z. Liu, "High mobility 2D palladium diselenide field-effect transistors with tunable ambipolar characteristics," Adv. Mater. **29**, 1602969 (2017).
[12]A. D. Oyedele, S. Yang, L. Liang, A. A. Puretzky, K. Wang, J. Zhang, P. Yu, P. R. Pudasaini, A. W. Ghosh, Z. Liu, C. M. Rouleau, B. G. Sumpter, M. F. Chisholm, W. Zhou, P. D. Rack, D. B. Geohegan, and K. Xiao, "$PdSe_2$: Pentagonal two-dimensional layers with high air stability for electronics," J. Am. Chem. Soc. **139**, 14090–14097 (2017).
[13]M. Long, Y. Wang, P. Wang, X. Zhou, H. Xia, C. Luo, S. Huang, G. Zhang, H. Yan, Z. Fan, X. Wu, X. Chen, W. Lu, and W. Hu, "Palladium diselenide long-wavelength infrared photodetector with high sensitivity and stability," ACS Nano **13**, 2511–2519 (2019).
[14]S. Zhang, J. Zhou, Q. Wang, X. Chen, Y. Kawazoe, and P. Jena, "Penta-graphene: A new carbon allotrope," Proc. Natl. Acad. Sci. **112**, 2372–2377 (2015).
[15]S. Liu, B. Liu, X. Shi, J. Lv, S. Niu, M. Yao, Q. Li, R. Liu, T. Cui, and B. Liu, "Two-dimensional penta-BP_5 sheets: High-stability, strain-tunable electronic structure and excellent mechanical properties," Sci. Rep. **7**, 2404 (2017).
[16]S. B. Desai, S. R. Madhvapathy, M. Amani, D. Kiriya, M. Hettick, M. Tosun, Y. Zhou, M. Dubey, J. W. Ager III, D. Chrzan, and A. Javey, "Gold-mediated exfoliation of ultralarge optoelectronically-perfect monolayers," Adv. Mater. **28**, 4053–4058 (2016).
[17]M. Amani, D.-H. Lien, D. Kiriya, J. Xiao, A. Azcatl, J. Noh, S. R. Madhvapathy, R. Addou, K. C. Santosh, M. Dubey, K. Cho, R. M. Wallace, S.-C. Lee, J.-H. He, J. W. Ager III, X. Zhang, E. Yablonovitch, and A. Javey, "Near-unity photoluminescence quantum yield in MoS_2," Science **350**, 1065–1068 (2015).
[18]O. S. Heavens, *Optical Properties of Thin Solid Films* (Dover, New York, 1991), pp. 55–59.
[19]P. Liu, P. Longo, A. Zaslavsky, and D. Pacifici, "Optical bandgap of single- and multi-layered amorphous germanium ultra-thin films," J. Appl. Phys. **119**, 014304 (2016).
[20]H. Zhang, Y. Ma, Y. Wan, X. Rong, Z. Xie, W. Wang, and L. Dai, "Measuring the refractive index of highly crystalline monolayer MoS_2 with high confidence," Sci. Rep. **5**, 8440 (2015).
[21]B. Radisavljevic and A. Kis, "Mobility engineering and a metal insulator transition in monolayer MoS_2," Nat. Mater. **12**, 815–820 (2013).
[22]S. Xu, Z. Wu, H. Lu, Y. Han, G. Long, X. Chen, T. Han, W. Ye, Y. Wu, J. Lin, J. Shen, Y. Cai, Y. He, F. Zhang, R. Lortz, C. Cheng, and N. Wang, "Universal low-temperature ohmic contacts for quantum transport in transition metal dichalcogenides," 2D Mater. **3**, 021007 (2016).
[23]M. Amani, C. Tan, G. Zhang, C. Zhao, J. Bullock, X. Song, H. Kim, V. R. Shrestha, Y. Gao, K. B. Crozier, M. Scott, and A. Javey, "Solution-synthesized high-mobility tellurium nanoflakes for short-wave infrared photodetectors," ACS Nano **12**, 7253–7263 (2018).
[24]M. Amani, E. Regan, J. Bullock, G. H. Ahn, and A. Javey, "Mid-wave infrared photoconductors based on black phosphorus-arsenic alloys," ACS Nano **11**, 11724–11731 (2017).
[25]X. Liu, H. Zhou, B. Yang, Y. Qu, and M. Zhao, "Strain-modulated electronic structure and infrared light adsorption in palladium diselenide monolayer," Sci. Rep. **7**, 39995 (2017).
[26]S. B. Desai, G. Seol, J. S. Kang, H. Fang, C. Battaglia, R. Kapadia, J. W. Ager, J. Guo, and A. Javey, "Strain-induced indirect to direct bandgap transition in multilayer WSe_2," Nano Lett. **14**, 4592–4597 (2014).
[27]X. Yu, P. Yu, D. Wu, B. Singh, Q. Zeng, H. Lin, W. Zhou, J. Lin, K. Suenaga, Z. Liu, and Q. J. Wang, "Atomically thin noble metal dichalcogenide: A broadband mid-infrared semiconductor," Nat. Commun. **9**, 1545 (2018).